DSM Generation and Interior Orientation Determination of IKONOS Images Using a Testfield in Switzerland

Emmanuel Baltsavias, Zhang Li, Henri Eisenbeiss

Institute of Geodesy and Photogrammetry, Swiss Federal Institute of Technology Zurich
ETH–Hoenggerberg, CH-8093 Zurich, Switzerland
E-mail: (manos, zhangl, ehenri)@geod.baug.ethz.ch

KEY WORDS: high-resolution satellite images, IKONOS, image matching, DSM generation, in-flight calibration, interior orientation

ABSTRACT:

We present processing of Ikonos triplet images over a testfield in Thun, Switzerland with accurate ground control points, 1600 m height range, variable land cover and suboptimal imaging conditions (snow, long shadows). A sophisticated matching algorithm for DSM generation is presented and the results are compared to reference data from airborne laser scanning. The RMS errors for the whole area, excluding vegetation, were 2-3 m, while for bare ground the accuracy is about 1 m or less. The accurate matching allowed the detection and quantification of errors in the interior orientation of the sensor, caused by changes in the relative position of the 3 CCDs forming the virtual CCD line. These errors were verified through a cooperation with Space Imaging and recomputation of the sensor interior orientation. The interior orientation errors caused height jumps of 1.3 to 1.5 m along two stripes at the overlap regions of the 3 CCDs. The method used for the detection and quantification of these errors is applicable for in-flight calibration of sensors forming a virtual image through butting of multiple CCD arrays, without the need of testfields with signalised points, which are difficult to establish and maintain. Depending on the accuracy of the matching method and of the reference DSM, we estimate that this in-flight calibration method can detect interior orientation errors causing parallax errors of 0.5 pixels or more.

1. INTRODUCTION

Linear CCD array sensors have been widely used to acquire panchromatic and multispectral images in pushbroom mode for photogrammetric and remote sensing applications. IKONOS, successfully launched on 24 September 1999, was the first civilian satellite with high-resolution sensors, acquiring panchromatic and multispectral images with 1-m and 4-m ground pixel size respectively. IKONOS can acquire two (stereo) or more images of the same region quasi simultaneously by agile pointing of the sensor through rotation of the satellite body, reducing thus the differences between these images and facilitating automated mensuration processes. This fact, together with the high spatial resolution of the images, the 11-bit quantization and the narrow field-of-view allows and requires an extension of the "classical" satellite image processing methods for the full exploitation of the potential of this data.

In recent years, a large amount of research has been devoted to the efficient utilization of these high spatial resolution images, e.g. regarding sensor modeling and image orientation (Baltsavias et al., 2001; Jacobsen, 2003; Grodecki and Dial, 2003; Fraser et al., 2002; 2003a; 2003b; Poli, 2004; Eisenbeiss et al., 2004a), automatic DSM/DTM generation (Toutin, 2004; Zhang and Gruen, 2004; Poon et al., 2005), feature extraction (Shan, 2003; Hu and Tao, 2003; Di et al., 2003; Baltsavias et al., 2004) and multi-channel color processing (Zhang, 2004; Hong and Zhang, 2004; Ranchin and Wald, 2000).

In this paper, we first briefly report about the key algorithms on automatic triangulation. Then, we present an advanced image matching method and give a detailed DSM accuracy evaluation using IKONOS *Geo*-level images in a testfield in Thun, Switzerland, with large height range and very variable terrain relief and land cover, and a laser DSM as reference data. The images were acquired at different times and pre-processed with different calibration parameters. Our matching method was developed for automatic DSM generation from linear array images and provides dense, precise, and reliable results. The approach uses a coarse-to-fine hierarchical solution with a combination of several image matching algorithms and automatic quality control. Finally, we reveal and quantify errors in the interior orientation of the sensor and present a general and practical method for in-flight calibration.

2. SENSOR MODELING AND BLOCK ADJUSTMENT

The imaging geometry of IKONOS is characterized by nearly parallel projection in along-track direction and perspective projection in cross-track direction. A rigorous model can be used to reconstruct the physical imaging geometry and to model transformations between object and image coordinate systems. Alternatively, Rational Function Models (RFMs) have recently drawn considerable interest in the remote sensing community. In particular, IKONOS is only supplied with rational polynomials coefficients (RPCs) instead of rigorous sensor model parameters, while RPCs are provided or can be derived for other optical satellite sensors as well. A RFM is generally the ratio of two polynomials derived from the rigorous sensor model and ground control and/or sensor orientation information. These models do not describe the physical imaging process but use a general transformation to describe the relationship between image and ground coordinates. If the RPCs are computed without Ground Control Points (GCPs) (as is the case, with the RPCs provided by Space Imaging (SI) for Ikonos), the geopositioning accuracy of the RPCs needs to be improved and a bias needs to be removed with a certain number of GCPs and an additional 2D transformation. For single typical size images, two translations are sufficient with Ikonos, while Quickbird exhibits more nonlinearities and requires a higher order transformation, e.g. affine (Eisenbeiss et al., 2004a). Grodecki and Dial (2003) proposed a method to block-adjust high-resolution satellite images described by RFMs and illustrated the method with IKONOS examples, suggesting the use of a linear scale factor in scanning direction when the image is long, e.g. over 50 km.

With the supplied RPCs, the mathematical model used is

$$\begin{aligned} x + \Delta x &= x + a_0 + a_1 x + a_2 y = RPC_x(\varphi, \lambda, h) \\ y + \Delta y &= y + b_0 + b_1 x + b_2 y = RPC_y(\varphi, \lambda, h) \end{aligned} \qquad (1)$$

where, a_0, a_1, a_2 and b_0, b_1, b_2 are the affine parameters for each image, and (x, y) and (j, l, h) the image and object coordinates of the points.

The block adjustment model expressed in equation (1) is justified for any photogrammetric camera with a very narrow field-of-view. Using this model, we expect that parameter b_0 is used to absorb all along-track errors causing offsets in the scanning direction, while parameter a_0 absorbs across-track errors causing offsets in the line CCD direction. Parameters b_1 and a_2 absorb shear effects caused by gyro drift during the image scan, while parameters a_1 and b_2 are used to absorb parts of the radial ephemeris error, and interior orientation errors such as focal length and a part of lens distortion errors. In our approach, we first used the RPCs to transform from object to image space and then using these values and the known pixel coordinates of GCPs we estimated either two translations (model M_RPC1) or all 6 affine parameters (model M_RPC2).

For satellite sensors with a narrow field of view like IKONOS, even simpler sensor models can be used, such as the 3D affine model (M_3DAFF) and the relief-corrected 2D affine (M_2DAFF) transformation. They are discussed in detail in Baltsavias et al. (2001) and Fraser et al. (2002). Their validity and performance is expected to deteriorate with increasing area size and rotation of the satellite during imaging (the so-called forward scanning mode) which introduces non-linearities, and for the 3D affine model with increasing height range and poor GCP distribution.

In order to apply the block adjustment, a certain number of GCPs and tie points have to be collected. In our approach, these points can be measured manually, semi-automatically or fully automatically. In particular, ellipse fitting and line intersection methods are suitable for GCP measurements over typical suburban, urban and rural areas (Fraser et al., 2002; Eisenbeiss et al., 2004a). In the experiments, these methods yielded suitable results for orientation of high-resolution satellite imagery. Examples of GCP measurements by using these 2 methods are shown in Fig. 1. Another technique of choice can be least squares template matching (Baltsavias et al., 2001).

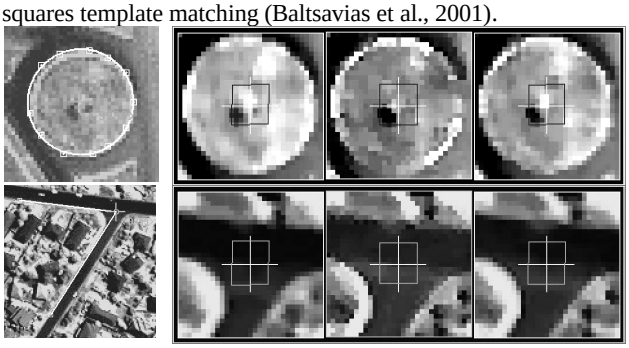

Fig. 1: GCP measurement in image space, where the point is determined by the ellipse fitting (upper) or line intersection method (lower) in one image (template image) and the conjugate points in the other images are computed with least squares matching.

3. THE MATCHING APPROACH

We have developed an image matching approach for automatic DSM generation from linear array images, which has the ability to provide dense, precise, and reliable results. The approach uses a coarse-to-fine hierarchical solution with a combination of several image matching algorithms and automatic quality control. The new characteristics provided by the linear array imaging systems, i.e. the multiple-view terrain coverage and the high quality image data, are also efficiently utilized in this approach.

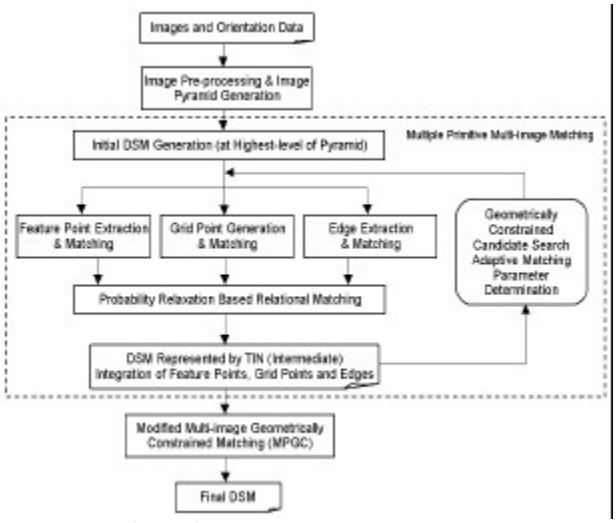

Fig. 2: Workflow of the automated DSM generation approach.

The approach essentially consists of several mutually connected components: the image pre-processing, the multiple primitive multi-image (MPM) matching, the refined matching and the system performance evaluation. The overall data flow of this matching approach is shown schematically in Fig. 2.The linear array images and the given or previously estimated orientation elements as used as input. After pre-processing of the original images and production of the image pyramids, the matches of three feature types (feature points, grid points and edges) in the original resolution images are found progressively starting from the low-density features in the lowest resolution level of the image pyramid. A TIN of the DSM is reconstructed from the matched features at each pyramid level by using the constrained Delauney triangulation method. This TIN in turn is used in the subsequent pyramid level for derivation of approximations and adaptive computation of some matching parameters. Finally, least squares matching is used to achieve more precise results for all matched features and for the identification of some false matches. The procedure is characterized by the following:

1) Multiple image matching: We do not aim at pure image-to-image matching, but seek instead image-to-object correspondences. We have developed a new flexible and robust matching algorithm – the Geometrically Constrained Cross-Correlation (GCCC) method in order to take advantage of the multiple images. The algorithm is based on the concept of multi-image matching guided from object space and allows reconstruction of 3D objects by matching all available images simultaneously, without having to match all individual stereo-pairs and merge the results.

2) Matching with multiple primitives: We have developed more robust hybrid image matching algorithms by taking advantage of both area-based matching and feature-based matching techniques and utilizing both local and global image information. In particular, we combine an edge matching method with a point matching method through a probability relaxation based relational matching process. The use of edges leads to preservation of surface discontinuities, while grid points bridge areas with little or no texture. One example of the edge matching is shown in Fig. 3. As it can be seen in the figure, even in areas of steep mountains there are many successfully matched line features, which are necessary for modeling of very rough and steep terrain.

3) Self-tuning matching parameters: The adaptive determination of the matching parameters results in higher success rate and less mismatches. These parameters include the size of the correlation window, the search distance and the correlation threshold values. This is done by analyzing the

matching results at the previous image pyramid level and using them at the current pyramid level.

4) High matching redundancy: With our matching approach, highly redundant matching results, including points and edges can be generated. Highly redundant matching results are suitable for representing very steep and rough terrain and allow the terrain microstructures and surface discontinuities to be well preserved. Moreover, this high redundancy also allows automatic blunder detection. Mismatches can be detected and deleted through analysis and consistency checking within a small neighbourhood of each match point.

5) Efficient surface modeling: The object surface is modeled by a triangular irregular network (TIN) generated by a constrained Delauney triangulation of the matched points and edges. A TIN is suitable for surface modeling because it integrates all the original matching results, including points and line features, without any interpolation. It is adapted to describe complex terrain types that contain many surface microstructures and discontinuities.

6) Coarse-to-fine hierarchical strategy: The algorithm works in a coarse-to-fine multi-resolution image pyramid structure, and obtains intermediate DSMs at multiple resolutions. Matches on low-resolution images serve as approximations to restrict the search space and to adaptively compute the matching parameters. The least squares matching methods are finally used to achieve sub-pixel accuracy for all matched features and identify some inaccurate and possibly false matches.

More details of this matching approach can be found in Gruen and Zhang (2003), Zhang and Gruen (2004) and Zhang (2005).

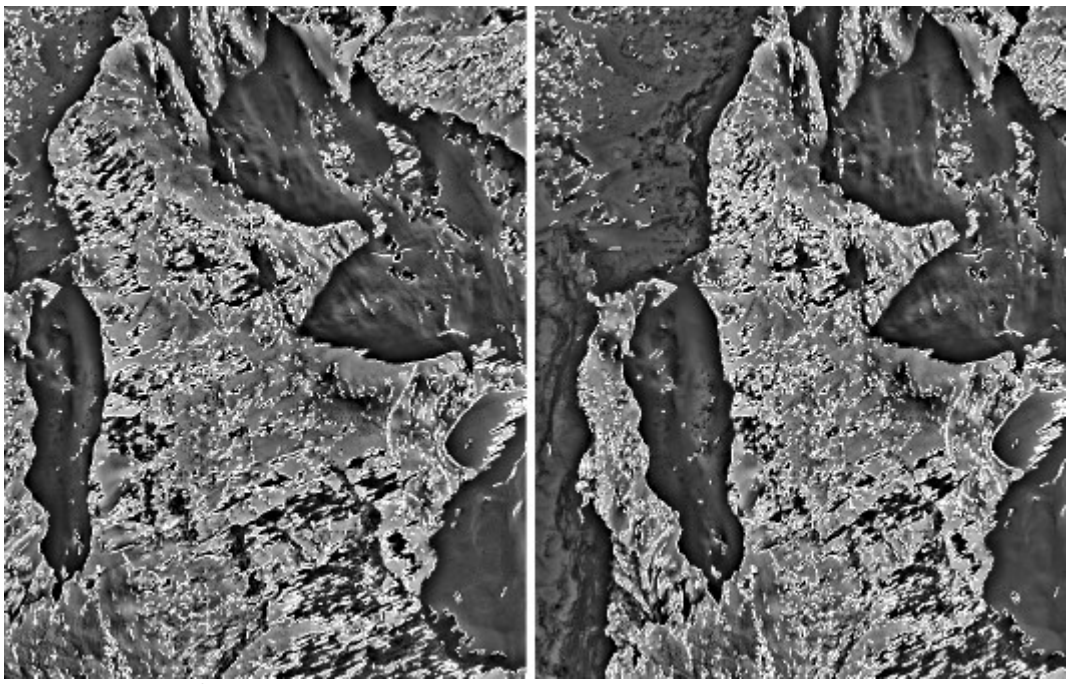

Fig. 3. Examples of edge matching with IKONOS images over rough and steep mountainous areas. The matched edges are shown in white and they are necessary for modeling this kind of terrain.

4. PERFORMANCE EVALUATION

The study site is an area around the town of Thun, Switzerland. This area consists of a steep mountainous region in the southwestern part and smooth hilly regions in the middle and northern parts. The town of Thun is located in the lower-middle part of the study area. The whole area is about 17×20 km^2 and 30% is covered by forests. The site has an elevation range of more than 1600 m (see shaded terrain model in Fig. 4) and the land cover is extremely variable.

Over this test area, three IKONOS image triplets (each covering ca. 11×20 km^2) were acquired, each triplet consisting of a stereopair and a nadir image. The first two image triplets (T_DEC_O and T_DEC_N) were acquired on the same day during winter time but were generated with different calibration parameters. These calibration parameters refer to the interior orientation of the sensor and allow an evaluation of the effect of interior orientation errors on DSM accuracy (see also section 5). In these two triplets, about 70% of the area was covered by snow, while sun elevation was very low (ca. 19°) causing long shadows and low contrast. Another triplet (T_OCT) was acquired during autumn with no snow, less shadows and better illumination conditions (Table 1). All IKONOS images were Geo, 11-bit, with DRA off, and 1m panchromatic (PAN) and 4m multi-spectral (MS) channels (for DSM generation only the PAN images were used). For all IKONOS images, the RPCs were provided in the metadata files.

Table 1: Main characteristics of the three IKONOS image triplets acquired over the study area.

Dataset	Image No.	Acquisition Date	Generation date	Sensor-Azimuth	Sensor-Elevation
T_DEC_O	135251_000	2003-12-25	2004-01-19	180.39°	62.95°
	135251_100	2003-12-25	2004-01-19	72.21°	82.15°
	135254_000	2003-12-25	2004-01-19	128.17°	82.62°
T_DEC_N	163001_000	2003-12-25	2005-03-02	180.39°	62.95°
	163001_100	2003-12-25	2005-03-02	72.21°	82.15°
	163003_000	2003-12-25	2005-03-02	128.17°	82.62°
T_OCT	157928_000	2003-10-12	2004-02-11	10.74°	77.85°
	157928_100	2003-10-12	2004-02-11	4.69°	85.26°
	157928_200	2003-10-12	2004-02-11	197.09°	71.95°

4.1 Block adjustment

In order to precisely georeference the IKONOS images, about 50 well-distributed GCPs were collected with differential GPS in March 2004. The measurement accuracy was about 0.25 m. As expected, GCPs were difficult to find in rural and mountainous areas, but also in the town of Thun, where they had to be visible in all images simultaneously. Shadows and snow made their selection even more difficult. As a result, only 39 of them could be measured precisely in the images. The GCPs were measured in one of images of each triplet (usually the nadir) by the line

intersection method and the conjugate points in the other images were computed with least squares matching.

Tables 2 and 3 compare the results of the orientation of the first two IKONOS triplets (T_DEC_O and T_DEC_N) with different sensor models and different number of GCPs. All methods achieved RMSE values in East (X) and North (Y) direction of about half a meter. The maximum residuals were about 1.0 m in planimetry and 2.0 m in height. However, the results of the second triplet that was generated with new calibration parameters were better than those of the first triplet, especially in the North direction, due to interior orientation errors in the T_DEC_O calibration (see also section 5). For the third triplet of T_OCT, it is not possible to make a comparison with the first two because in this triplet almost 50% of the area (northern part) was covered by clouds resulting in a different number and distribution of GCPs. However, even with the GCPs and check points (CPs) measured in the southern part of the images, the RMSE (M_RPC1) of the orientation was 0.30 m in East, 0.54 m in North and 0.77 m in height.

The results show that decreasing the number of GCPs down to 5 did not decrease the accuracy significantly, and that sub-meter accuracy can be achieved using only a few GCPs and the RPC or the 3D affine (M_3DAFF) model. For more detailed block adjustment results with different IKONOS datasets and different GCP distributions, see Eisenbeiss et al. (2004a, 2004b).

Table 2: Comparison of sensor models and number of GCPs for the IKONOS triplet (T_DEC_O). CPs are check points.

Sensor Model	GCPs (CPs)	X-RMSE (max. error) [m]	Y-RMSE (max. error) [m]	Z-RMSE (max. error) [m]
M_RPC2	22 (0)	**0.32** (0.70)	**0.78** (1.53)	**0.55** (0.78)
M_RPC2	18 (4)	**0.33** (0.80)	**0.79** (1.48)	**0.56** (1.41)
M_RPC2	12 (10)	**0.32** (0.73)	**0.82** (1.64)	**0.60** (1.04)
M_RPC2	5 (17)	**0.44** (1.04)	**0.92** (1.83)	**0.65** (1.15)
M_RPC1	22 (0)	**0.35** (0.82)	**0.41** (0.91)	**0.67** (0.80)
M_3DAFF	22 (0)	**0.32** (0.73)	**0.78** (1.50)	**0.55** (0.78)

Table 3: Comparison of sensor models and number of GCPs for the IKONOS triplet (T_DEC_N). CPs are check points.

Sensor Model	GCPs (CPs)	X-RMSE (max. error) [m]	Y-RMSE (max. error) [m]	Z-RMSE (max. error) [m]
M_RPC2	22 (0)	**0.37** (0.70)	**0.32** (0.79)	**0.48** (1.07)
M_RPC2	18 (4)	**0.38** (0.79)	**0.33** (0.75)	**0.50** (0.98)
M_RPC2	12 (10)	**0.40** (0.92)	**0.35** (0.85)	**0.69** (1.66)
M_RPC2	5 (17)	**0.45** (1.08)	**0.43** (0.96)	**0.76** (1.86)
M_RPC1	22 (0)	**0.37** (0.76)	**0.34** (0.66)	**0.64** (1.26)
M_3DAFF	22 (0)	**0.43** (0.89)	**0.53** (0.90)	**0.76** (1.83)

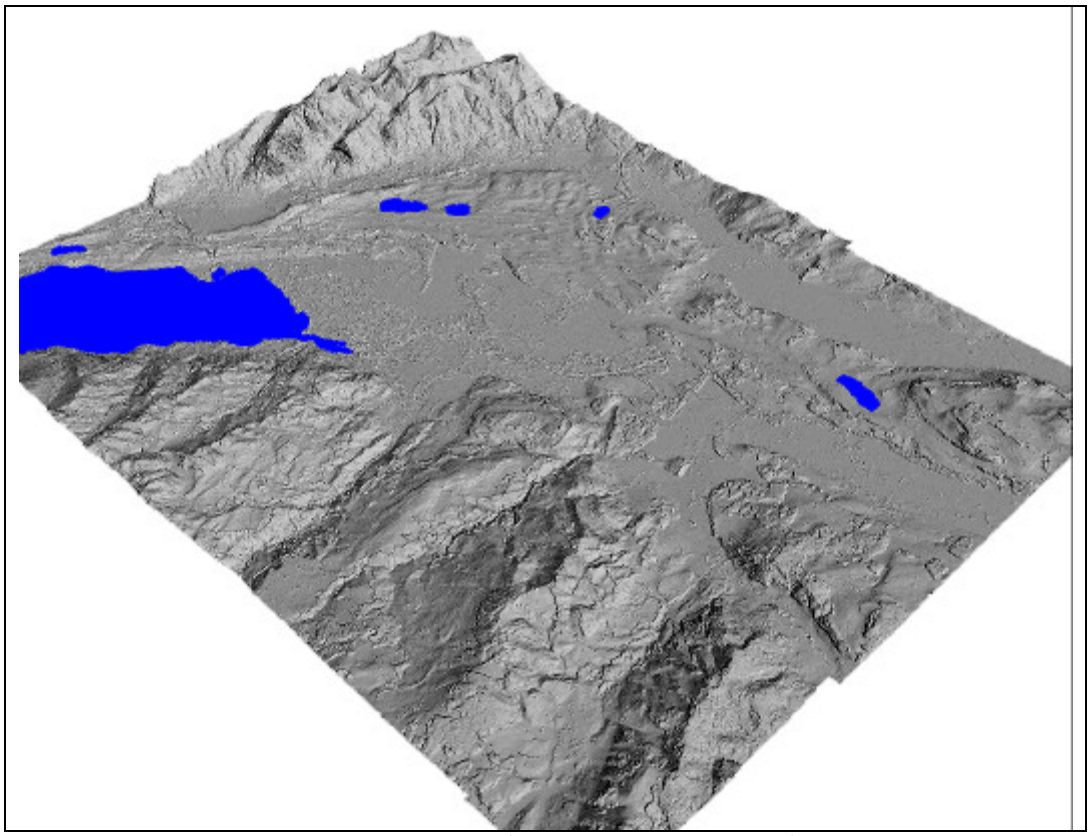

Fig. 4: Shaded terrain model (5 m grid spacing) of the whole study area (seen from the North) generated by image matching and the triplet - T_DEC_N.

4.2 DSM generation and evaluation

In order to quantitatively evaluate the accuracy of the generated DSM, a 2m irregular-spacing laser DSM, with an accuracy of 0.5 m (1σ) for bare ground areas and 1.5 m for vegetation areas, was used as reference data. The laser DSM was acquired in the year 2000 and provided by the Swiss Federal Office of Topography, Bern (Swisstopo). It only covers the southern part of the study area.

After all IKONOS image triplets were preprocessed by using the algorithms proposed in Baltsavias et al. (2001) and the same parameters, our matching approach was applied. The three images of each triplet were matched simultaneously in order to achieve more reliable results. Some areas like lakes and rivers were manually defined as “dead areas” via a user-friendly interface and were excluded from matching. Taking the triplet T_DEC_N as an example, the matching approach resulted in ca.

11 million points and 800,000 edges, of which more than 80% were labeled as highly reliable (quality indicator > 0.75).

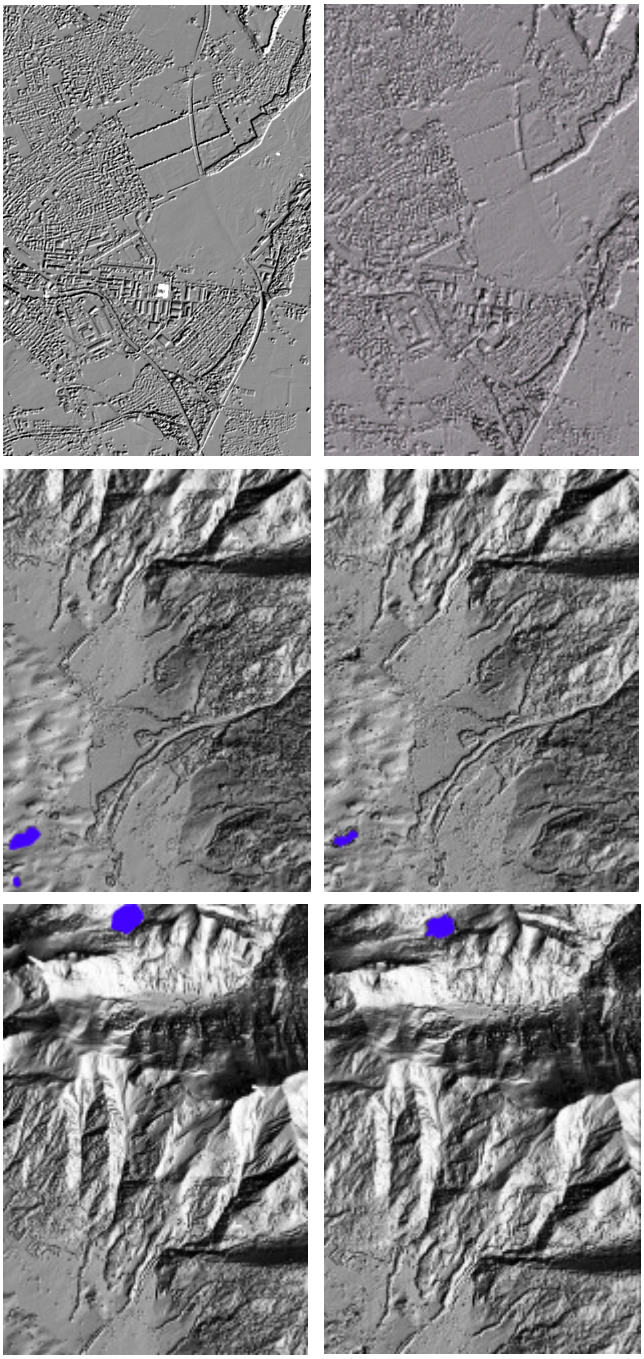

Fig. 5: Shaded terrain models of three sub-areas, where the lower one shows the mountain area, the middle one vegetation areas and the upper one the area around the town of Thun. Left: Laser DSM (2 m average pint distance); Right: results of matching from the T_OCT triplet.

Finally, three 5m regular grid DSMs were interpolated from the raw matching results. Fig. 4 shows the shaded terrain model for the whole study area and Fig. 5 shows a comparison of the laser DSM and the results of matching for three sub-areas. As it can be seen, the resulting DSM reproduced quite well not only the general features of the terrain relief but also small geomorphological and other features visible in the IKONOS images. The resulting DSM showed many topographic details and different features, like small valleys in the mountains, detailed patterns related to streets and buildings in suburban and urban areas, linear features related to highways and main road networks, sparse trees, small clusters of houses and forest areas.

Table 4: DSM accuracy evaluation results (in m) for the triplet T_DEC_O, where, B1 – Bare ground; B2 – Bare ground (including mountainous area); B3 – Bare ground (including mountainous and shadow areas); C – City area only; V – Vegetation area only; W1 – Whole area; W2 – Whole area without vegetation areas. RMSE (95) and Average (95) are the RMS and average (signed) height difference values after excluding the 5% largest differences.

Terrain type	No. of compared points	RMSE	Average	RMSE (95)	Average (95)
B1	7,037,578	1.27	0.82	0.93	0.89
B2	7,993,875	1.84	0.92	1.04	0.92
B3	9,763,257	2.11	0.80	1.20	0.80
C	2,794,389	3.34	0.30	2.36	0.30
V	8,689,642	8.16	1.68	-	-
W1	28,854,764	4.93	1.13	4.24	1.14
W2	18,022,149	2.74	0.70	1.45	0.69

Table 5: DSM accuracy evaluation results (in m) for the triplet T_DEC_N.

Terrain type	No. of compared points	RMSE	Average	RMSE (95)	Average (95)
B1	7,037,578	1.15	0.31	0.73	0.37
B2	7,993,875	1.90	0.34	0.93	0.35
B3	9,763,257	2.14	0.29	1.19	0.30
C	2,794,389	3.38	0.51	2.41	0.51
V	8,689,642	8.05	1.58	-	-
W1	28,854,764	4.90	0.50	4.23	0.50
W2	18,022,149	2.54	0.35	1.41	0.34

Table 6: DSM accuracy evaluation results (in m) for the triplet T_OCT.

Terrain type	No. of compared points	RMSE	Average	RMSE (95)	Average (95)
B1	7,037,578	1.41	0.22	0.95	0.21
B2	7,993,875	1.77	0.29	1.09	0.29
B3	9,763,257	1.75	0.29	1.07	0.29
C	2,794,389	2.83	-0.25	2.08	-0.25
V	8,689,642	6.61	-1.97	-	-
W1	28,854,764	4.25	-0.40	2.96	-0.39
W2	18,022,149	2.05	0.16	1.32	0.16

A quantitative evaluation of the DSM was conducted by comparison with the laser DSM and nearly 28 million elevation points were used in statistical computations for the whole study area. We show here the results of the raw computations, without any a posteriori manual editing procedure applied. Tables 4 to 6 give the DSM accuracy evaluation results. We computed the differences as reference DSM minus the interpolated heights from our generated DSM. The accuracy of the generated DSM, excluding vegetation areas, is between 1.0 – 5.0 m, depending on the terrain relief and land cover. The results can be summarized as follows:

- High accuracy at meter or even sub-meter level can be achieved in bare ground areas. We could not select truly bare ground areas, instead our areas still contain many sparse trees and small clusters of houses. The analysis shows that in bare ground areas more than 70 percent of the points have differences of less than 1m. Around the areas of sparse trees and small

houses, the resulting DSM is lower than the laser DSM. This can be expected because usually these small features were either smoothed out by our matching method or removed in the automated blunder detection procedure.

- A bias of about 1.0-1.5 m can be observed in the T_DEC_O results caused mainly by interior orientation errors. A part of the differences is also due to the 3 years difference between acquisition of the laser DSM and the Ikonos images, and regarding the vegetation due to the different state of the trees (in the October triplet with leaves, in the December ones without).
- In urban and forest areas the accuracy becomes worse, which is due to the fact that the reference laser measurements and the DSM determined in matching may refer to partly different objects. Usually, the generated DSM is higher than the laser DSM in forest areas (laser can sometimes penetrate the tree canopy) and narrow low-lying objects (like streets in very dense residential areas). However, for large buildings, the two DSMs coincided quite well.
- Other factors that influenced the matching were the long and strong shadows and occlusions, especially in the mountain areas, and very low textured snow areas. However, after our particular preprocessing the long and strong shadows are good for DSM generation in bare ground areas because they seem to generate more image texture information with less noise.
- In steep mountain areas (slope more than 70°), there are also some blunders with more than 400 m height difference. They are mainly caused by occlusions. In addition, the smoothness constraints smoothed out some steep and small features of the mountain areas (mainly in shadow areas) because there were not enough extracted and matched edges.
- In addition, the difference values show some stripe-like patterns for triplet T_DEC_O and T_OCT (Fig. 6). In these stripes, the height difference values show a jump of about 1.3-1.5 m. These patterns, however, do not appear in the dataset of T_DEC_N (Fig. 7). The reason for these stripes is explained in section 5.

Taking all above factors into account, it becomes clear that IKONOS has a very high geometric accuracy potential and with sophisticated matching algorithms a height accuracy of around 1.0 m can be achieved in bare ground areas.

5. IN-FLIGHT CALIBRATION AND DETERMINATION OF INTERIOR ORIENTATION PARAMETERS

In-flight calibration is important for satellite sensors, since during launch the environmental conditions change rapidly and drastically and this usually causes changes in the internal sensor geometry, which is determined in a pre-launch calibration. Furthermore, when the camera is large some of the interior orientation parameters can not ne determined with a laboratory calibration (Space Imaging, personal communication). The environmental conditions after orbit stabilisation are also harsh and may cause internal geometry changes, however this is not as crucial as the changes that occur during launch. For these reasons, an inflight-calibration is usually a must and companies operating satellites take measures to perform such calibration, sometimes with the use of testfields and many accurate, often signalised GCPs. The establishment and maintenance of such testfields is difficult and costly. Inflight-calibration may not permit the determination of all internal geometry sensor parameters. This is even more the case with high-resolution satellites, like Ikonos, with a very narrow field-of-view and many internal geometry parameters and a complicated focal plane arrangement of multiple CCD linear arrays. In this case, many of the sensor parameters are highly correlated and not determinable. One may argue, that with the help of GCPs and use of RPCs, errors in the interior orientation parameters are absorbed without any negative effect in the determination of planimetric and 3D coordinates of ground points. However, as we will show below, some possible interior orientation errors, can not be modelled by RPCs and can decrease the accuracy of 3D point positioning significantly. This is a problem for applications requiring very high accuracy, exploiting the full accuracy potential of satellites like Ikonos and Quickbird which lies in the 3-4 dm and 5-6 dm level for planimetry and height respectively (Fraser et al., 2002).

The design of the Ikonos focal plane is quite complicated. It consists of two TDI panchromatic CCD arrays, one for reverse and one for forward mode scanning, the TDI having 32 stages. Furthermore, there are 4 multispectral arrays, without TDI. Each of the 2 panchromatic and 4 multispectral arrays consists actually of 3 separate CCDs that are mechanically butted to form a long line. The reason for use of 3 CCDs is either that at the time of the sensor production a single CCD with that length was not possible, or that Kodak prefered for production speed, cost and reliability reasons to use standard, off-the-shelf tried components. This sensor design is mentioned, although sometimes vaguely, in few SI papers, but it is not widely known. The length of each of the 3 CCDs is unknown, but we estimate it, based on a published photograph, to be about 5,000 pixels, allowing an overlap between the 3 CCDs of sufficient width. The central of the 3 CCDs is offset from the other two in the direction vertical to the CCD lines, while in the CCD line direction, the central CCD overlaps with the other two. This overlap allows radiometric and geometric corrections when stitching the 3 CCD line images to one. It is unknown whether SI performs geometric corrections, e.g. by matching corresponding points in the overlap region and adjusting the geometry of the partial images, although this seems rather not be the case, as the problems mentioned below imply. Radiometric corrections are apparently performed. If the geometry of these 3 CCD lines is known and stable, then stitching the 3 images together should not be a problem. However, due to changes in the internal sensor geometry during and after launch, as mentioned above, the relative geometry of the 3 CCDs forming one virtual long line will not remain stable. Various deformations (shifts, rotations, etc.) may occur in the focal plane and out-of-plane, the most probable ones being shifts and rotations in plane. Such problems may occur not just with Ikonos, but any sensor forming a virtual line from multiple single CCD lines, and independently of the way the CCDs are butted (optically, mechanically, through use of multiple lenses etc.). For Quickbird, possible errors are even more, since this sensor has a similar focal plane geometry as Ikonos, but with 6 CCDs (instead of 3) forming the virtual CCD line. The 6 partial CCD images are obvious in many quicklooks in the Digital Globe archive, due to radiometric differences between them. Again the fact that Quickbird uses 6 CCDs to form a line is not widely known. For both Quickbird and Ikonos, the RPCs are computed for a whole image formed by the virtual CCD line, and thus deformations of the single CCDs can not be modelled.

First DSM accuracy analysis and visualisation of errors using the Thun testfield showed the stripes of Fig. 6. The average height jump at profiles P3 and P4 was 1.5 m and at P1 and P2 1.3 m, corresponding to a parallax error in y (scanning direction) of about 0.7-0.8 pixels, while the x-parallax error was only 0.15-0.2 pixels. A first thought was that these stripes could be due to laser scanner errors. Neighbouring laser scanner strips may exhibit offsets, tilts etc., if the strips are not tied together appropriately in a common adjustment. This was even more probable as the Thun region was the very first region in Switzerland that was covered with laser scanner data and at that initial stage the Swisstopo but also the companies performing the data collection, processing and editing had relatively little experience. The Thun region, among all Swiss territory covered with laser scanner

data, is estimated by the Swisstopo to be the region with the least accurate laser DSM. However, the distance between the stripes observed in Fig. 6 was too large compared to the laser scanner swath, and the fact that they were two, and approximately at the overlap regions of the 3 CCDs was quite suspicious. To verify the assumption of interior orientation errors of the Ikonos sensor, the following procedure was followed. First, the Ikonos quicklooks were used to find the approximate position of the overlap regions (and possible seam lines between the 3 CCDs). The quicklooks are the raw data, after stitching, with a spatial resolution of about 16 m. Then, these regions were transferred to the Geo images using corresponding points. Next, we identified areas that were almost totally flat in these overlap regions. We then matched semi-automatically with least squares matching in the Geo forward and backward images of the stereopair of the triplet T_DEC_O very dense points along a profile that was vertical to each of the two overlapping regions (stripes). In these flat regions, interior orientation errors were visible as parallax jumps along the profiles. The position of these jumps allowed us to estimate the number of pixels, been used from each of the 3 CCDs to form the virtual line, this number being about 4,624 pixels with a feathering zone of about 24 pixels. The overlap regions were estimated to be about 200 pixels wide. The fact that errors appear only at the overlap regions is easily understandable. A shift, e.g. in the middle of the 3 CCDs, will be stable during the quasi-simultaneous image acquisition of a stereopair or triplet, and thus for object points imaged at the same CCD no y-parallax (in the scanning direction) will be introduced (the planimetric position of such points will be shifted, but their height will be similar apart from positions of abrupt height discontinuities). However, ground points imaged at different CCDs will exhibit parallax (and height) errors. This will always happen as the pointing accuracy of Ikonos on the rgound is in the order of few hundred meters. The above procedure is not optimal as a) it requires flat regions and b) matching errors along one single profile, due e.g. to lack of texture, may cause parallax jumps. A more appropriate in-flight calibration procedure will be outlined below.

This procedure uses the very dense matching results and their differences from the reference data (laser DSM) in open, not rugged areas, ideally with enough texture to allow accurate matching. Thus, areas with trees, bushes, urban areas etc. were excluded, and areas shown at the position of profiles P1 to P4 (see Fig. 6) were selected. These profiles can actually be rectangular areas along the stripes to allow a high number of height differences to be used in the further analysis. The high number allows a smoothing of matching errors and errors of the reference data and also an elimination of large differences due to few single trees and buildings included in the rectangle. As already mentioned, the accuracy of our matching algorithm in open terrain is 1 m or less. Through averaging of many height differences, we anticipate to estimate the height jump with an accuracy 0.3-0.5 m, depending also on the quality of the reference data. At the position of each profile the height jump at the left and right side of each profile is computed through averaging of values to the left and right side of each jump. The estimation of the jump at the left and right part of each profile and especially the comparison between the jump in the left and right overlap regions allows to estimate whether there is only a shift between the 3 CCDs or also a rotation. The above procedure can be used as a general in-flight calibration method to determine such interior orientation errors. The reference data may come from any source and should have an accuracy of a few dms. In this respect, the laser data used here were not optimal, as their accuracy (one sigma) at open terrain was 0.5 m and they had some artifacts (see below). The terrain does not have to be flat (undulating terrain is fully sufficient), while no signalised points are needed. The same area can be used many times and with different sensor azimuth and elevation, and scanning mode configurations to allow a more reliable estimation of interior orientation errors and their better separation, if multiple errors (shifts and rotations) exist.

The above analysis with the T_DEC_O was made in April 2004 but was not published for various reasons. After personal contacts with SI and verification of the encountered problems, SI performed a new more accurate determination of the Ikonos internal geometry, and the December 25th images were processed with this new calibration (T_DEC_N), while the October images were still with the old calibration. It is unknown how this new calibration was performed by SI. A comparison of Figs. 6 and 7 shows a significant improvement with the new calibration and no apparent stripes and height jump in Fig. 7. It also stresses the importance of performing a frequent in-flight calibration by the companies operating satellites. The influence of the new calibration on the 3D positioning accuracy is also shown in the Y-RMSE values of Tables 2 and 3 and the average error values of Tables 4 and 5. An analysis of the October images showed a jump at both overlap regions, however, the width of the jump was smaller. The width of the overlap depends on the number of ground points imaged by different CCD lines (out of the 3), and thus on the parameters of the images, especially the scanning azimuth and the overlap of the images. It is also influenced by scale differences between the images, the stripes becoming more apparent when the scale differences increase (which is the case when the stereopair images are not symmetric with respect to the nadir).

The differences between laser DSM and the matching results of all triplets showed some systematic artifacts, see arrows in Fig. 7. These are attributed to errors in the laser DSM. It is scientifically very interesting to see that sophisticated matching methods and satellite images from 680 km flying height can reveal errors in airborne laser scanning, although this is certainly not a cost-effective method for quality control of DSMs generated by laser scanning.

Similar tests with a Quickbird stereopair were attempted, however the imaged area was almost totally covered by forests and thus possible interior orientation errors were not apparent.

6. CONCLUSIONS

We presented processing of Ikonos triplet images over a testfield in Thun, Switzerland with accurate ground control points, 1600 m height range, variable land cover and suboptimal imaging conditions (snow, long shadows). A sophisticated matching algorithm for DSM generation was presented and the results were compared to reference data from airborne laser scanning. The RMS errors for the whole area, excluding vegetation, were 2-3 m, while for bare ground the accuracy is about 1 m or less. As evidenced by the visual inspection of the results, our matching method can reproduce not only the general features of the terrain relief, but also detailed features of relief. The results were partly influenced by the suboptimal accuracy of the reference DSM and its temporal difference from the acquisition of the Ikonos images. The largest errors usually occurred in the shadow, tree and building covered areas and the best results were obtained in bare ground areas. If the bias introduced by trees and buildings is taken out, we can expect a height accuracy of one pixel or even better from IKONOS imagery as “best case” scenario. A major problem of our automatic DSM generation approach is the automated detection of small blunders, which still exist in the results. This constitutes a relevant topic for further research.

The accurate matching allowed the detection and quantification of errors in the interior orientation of the sensor, caused by

changes in the relative position of the 3 CCDs forming the virtual CCD line. These errors were verified through a cooperation with Space Imaging and recomputation of the sensor interior orientation. The interior orientation errors caused height jumps of 1.3 to 1.5 m along two stripes at the overlap regions of the 3 CCDs. The method used for the detection and quantification of these errors is applicable for in-flight calibration of sensors forming a virtual image through butting of multiple CCD arrays, without the need of testfields with signalised points, which are difficult to establish and maintain. Depending on the accuracy of the matching method and of the reference DSM, we estimate that this in-flight calibration method can detect interior orientation errors causing parallax errors of 0.3-0.5 pixels or more.

ACKNOWLEDGEMENTS

We acknowledge the support of Space Imaging USA by provision of the images and fruitful discussions and the support of the Swiss Federal Office of Topography, Bern, which provided the laser DSM.

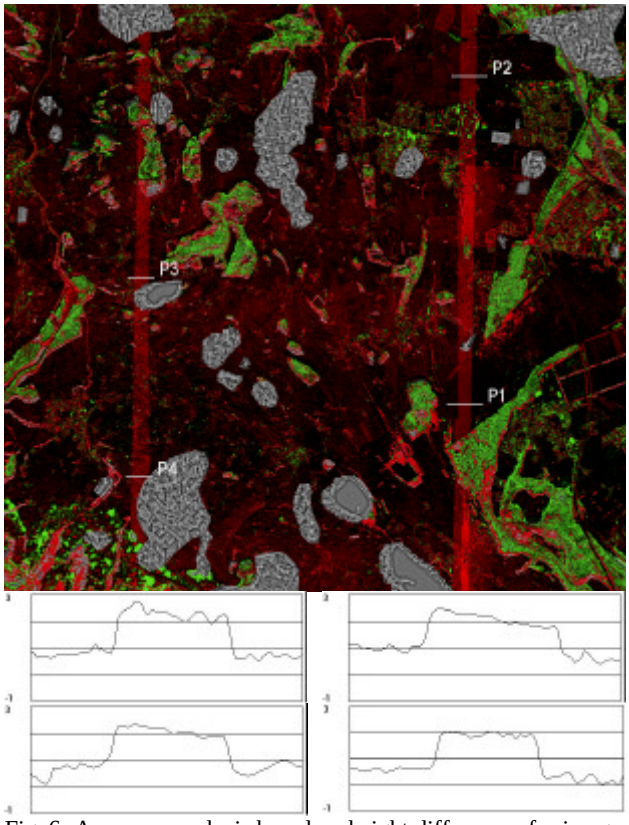

Fig. 6: Accuracy analysis based on height differences for image triplet T_DEC_O. Top: the 2D distribution of the height differences (in green and red negative and positive values, respectively). The following bar shows the color coding of the difference values). The height differences were computed from the reference DSM and the interpolated heights from the DSM from matching. Bottom: the height differences along 4 profiles (P1 to P4).

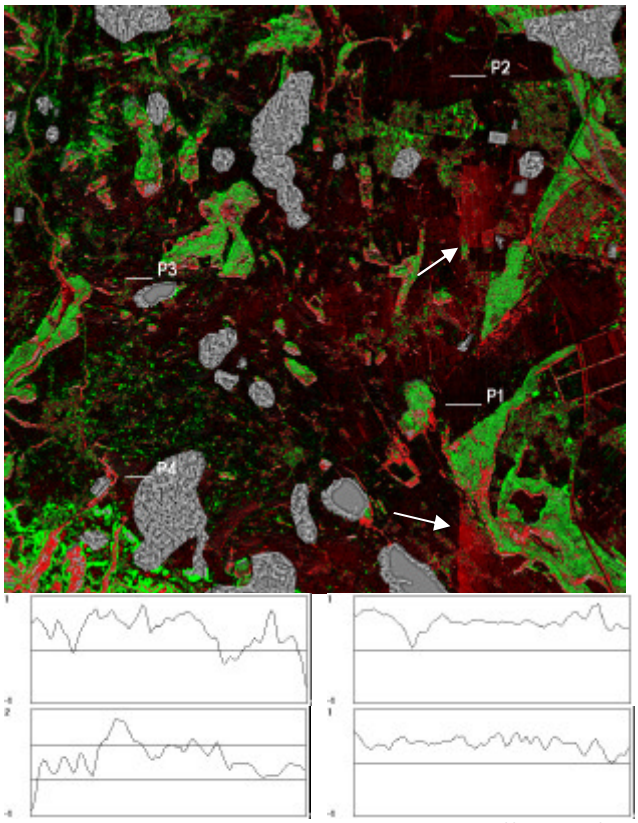

Fig. 7: Accuracy analysis based on terrain height differences for image triplet T_DEC_N. Top: the 2D distribution of the height differences (in green and red negative and positive values, respectively). The following bar shows the color coding of the difference values). The height differences were computed from the reference DSM and the interpolated heights from the DSM from matching. Bottom: the height differences along 4 profiles (P1 to P4).

REFERENCES

Baltsavias, E. P., O'Sullivan, L., Zhang, C. (2004). Automated Road Extraction and Updating using the ATOMI System – Performance Comparison between Aerial Film, ADS40, IKONOS and QuickBird Orthoimagery. *IAPRS, Vol. 35* (B4): 1053-1058.

Baltsavias, E. P., Pateraki, M., Zhang, L. (2001). Radiometric and Geometric Evaluation of IKONOS Geo Images and Their Use for 3D Building Modeling. *Joint ISPRS Workshop on "High Resolution Mapping from Space 2001", Hannover, Germany, 19-21 September* (on CD-ROM).

Di, K., Ma, R., Li, R. (2003). Automatic Shoreline Extraction from High-resolution IKONOS Satellite Imagery. *Proceedings of ASPRS 2003 Conference, Anchorage, Alaska, May 5-9* (on CD-ROM).

Eisenbeiss, H., Baltsavias, E. P., Pateraki, M., Zhang, L. (2004a). Potential of IKONOS and QUICKBIRD Imagery for Accurate 3D-Point Positioning, Orthoimage and DSM Generation. *IAPRS, Vol. 35* (B3): 522-528.

Eisenbeiss, H., Baltsavias, E. P., Pateraki, M., Zhang, L., Gut, O., Heller, O. (2004b). Das Potenzial von IKONOS- und QuickBird-Bildern fuer die genaue 3D-Punktbestimmung, Orthophoto- und DSM-Generierung. *Geomatik Schweiz*, (9): 556-562.

Fraser, C., Baltsavias, E. P., Gruen, A. (2002). Processing of IKONOS Imagery for Sub-meter 3D Positioning and Building Extraction. *ISPRS Journal of Photogrammetry & Remote Sensing, 56*(3): 177-194.

Fraser, C., Hanley, H. B. (2003a). Bias Compensation in Rational Functions for IKONOS Satellite Imagery. *Photogrammetric Engineering and Remote Sensing, 69*(1): 53-57.

Fraser, C., Yamakawa, T. (2003b). Applicability of the affine model for IKONOS image orientation over mountainous terrain. *Joint ISPRS/EARSL Workshop on High-Resolution Mapping from Space 2003, Hannover, Germany, 6-8 October* (on CD-ROM).

Gruen, A., Zhang, L. (2003). Automatic DTM generation from TLS data. *Optical 3-D Measurement Techniques VI, Vol. I*, pp. 93-105.

Gruen, A., Remondino, F., Zhang, L. (2004). 3D Modeling and Visualization of Large Cultural Heritage Sites at Very High Resolution: The Bamiyan Valley and Its Standing Buddhas. *IAPRS, Vol. 35*(B5): 522-528.

Grodecki, J., Dial, G. (2003). Block Adjustment of High-Resolution Satellite Images Described by Rational Polynomials. *Photogrammetric Engineering and Remote Sensing, 69*(1): 59-68.

Hong, G., Zhang, Y. (2004). The Effects of Different Types of Wavelets on Image Fusion. *IAPRS, Vol. 35 (B4):* 915-920.

Hu, X., Tao, C. V. (2003). Automatic Extraction of Main-Road Centerlines from IKONOS and Quick-Bird Imagery Using Perceptual Grouping. *Proc. ASPRS 2003 Conference, Anchorage, Alaska, May 5-9* (on CD-ROM).

Jacobsen K. (2003). Geometric Potential of IKONOS- and QuickBird-Images. *In: D. Fritsch (Ed.), Photogrammetric Weeks '03*, pp. 101-110.

Poli, D. (2004). Orientation of Satellite and Airborne Imagery from Multi-line Pushbroom Sensors with a Rigorous Sensor Model. *IAPRS, Vol. 35*(B1): 130-135.

Poon, J., Fraser, C., Zhang, C., Zhang, L., Gruen, A. (2005). Quality Assessment of Digital Surface Models Generated from IKONOS Imagery. *Photogrammetric Record* (submitted)

Ranchin, T., Wald, L. (2000). Fusion of High Spatial and Spectral Resolution Images: The ARSIS Concept and its Implementation. *Photogrammetric Engineering and Remote Sensing*, 66(1): 49-61.

Shan, J. (2003). On the Quality of Automatic Building Extraction from IKONOS Imagery. *Proc. ASPRS 2003 Conference, Anchorage, Alaska, May 5-9* (on CD-ROM).

Tao, C. V., Hu, Y. (2001). A Comprehensive Study of the Rational Function Model for Photogrammetric Processing. *Photogrammetric Engineering and Remote Sensing, 66*(12): 1477-1485.

Toutin, Th. (2004). Comparison of Stereo-Extracted DTM from Different High-Resolution Sensors: SPOT-5, EROS-A, IKONOS-II, and QuickBird. *IEEE Transactions on Geoscience and Remote Sensing, 42*(10): 2121-2129.

Zhang, L., Gruen, A. (2004). Automatic DSM Generation from Linear Array Imagery Data. *IAPRS, Vol. 35*(B3): 128-133.

Zhang, L. (2005). Automatic Digital Surface Model (DSM) Generation from Linear Array Images. *Ph. D. dissertation Institute of Geodesy and Photogrammetry, ETH Zurich, Switzerland* (submitted).

Zhang, Y. (2004). Problems in the Fusion of Commerial High-resolution Satellite as well as Landsat7 Images and Initial Solutions. *URL: http://www.isprs.org/commission4/ proceedings/pdfpapers/220.pdf*